arXiv:1211.4006v1 [cond-mat.mtrl-sci] 16 Nov 2012

High three dimensional thermoelectric performance from low dimensional bands

David Parker, Xin Chen and David J. Singh
Materials Science and Technology Division, Oak Ridge National Laboratory, 1 Bethel Valley Rd., Oak Ridge, TN 37831-6056
(Dated: November 19, 2012)

Reduced dimensionality has long been regarded as an important strategy for increasing thermoelectric performance, for example in superlattices and other engineered structures. Here we point out and illustrate by examples that three dimensional *bulk* materials can be made to behave as if they were two dimensional from the point of view of thermoelectric performance. Implications for the discovery of new practical thermoelectrics are discussed.

INTRODUCTION

Thermoelectric performance is quantified by the figure of merit, $ZT = \sigma S^2 T/\kappa$, where σ is the electrical conductivity, κ is the thermal conductivity, S is the thermopower (Seebeck coefficient) and T is the absolute temperature. [1, 2] There is no known thermodynamic or other fundamental limitation on ZT, but finding high ZT materials is very challenging and only a handful of materials with ZT significantly higher than unity are known. The difficulty is that finding high ZT requires finding a material that combines transport properties that do not normally occur together. Here we focus on the combination of high thermopower and high conductivity.

The low T electrical conductivity of a metal or degenerate semiconductor depends on the electronic states and their scattering at the Fermi level, E_F, specifically $\sigma \propto N(E_F) < v^2 > \tau$, where N is the density of states, $< v^2 >$ is the average Fermi velocity for the current direction, and τ is an inverse scattering rate. [3, 4] At finite temperature the expressions are similar but are integrated with the derivative of the Fermi function, which amounts to a temperature broadening. The conductivity therefore improves as one moves E_F away from the band edge, as in that case both the velocity and $N(E_F)$ increase. The thermopower is different. At low T, $S(T) \propto T(d\sigma/dE)/\sigma$, i.e. S/T is large near the band edge where the logarithmic derivative of σ with energy is high.

Hicks and Dresselhaus suggested that this conundrum could be overcome in quantum well structures. [5] They observed that in a two dimensional system the dependence of the density of states on energy for a parabolic band is a step function, meaning that for the in-plane direction one may expect a faster onset of the conductivity with energy and furthermore that S will be higher for a given carrier concentration. Viewed in three dimensions, the Fermi surfaces of superlattices or two dimensional semiconductors are in the shape of cylinders or pipes running along the direction of the layering rather than the spheres or ellipsiods of three dimensional doped semiconductors.

However, most applications of thermoelectrics involve macroscopic devices that are difficult to implement with superlattices and additionally, there can be problems such as parasitic heat conduction in barrier layers of superlattices. Nonetheless, it is interesting to observe that Na_xCoO_2, which is representative of the highest performance oxide thermoelectrics, and has high ZT at high carrier concentration, [6] has a very two dimensional electronic structure. [7] This material illustrates another problem with using 2D electronic systems as thermoelectrics. The high electrical conductivity is realized only in the layers, not perpendicular to them, while the heat conduction is more isotropic. As such, the very high ZT is realized only in single crystals for in-plane conduction or at least in highly textured ceramic. Here we propose an alternate resolution of the conundrum of high σ and high S using low dimensional electronic structures.

We observe that it is possible to have an electronic structure that is low dimensional in a material that is not low dimensional provided that symmetry is obeyed. This is known in metallic materials, the best example being body centered cubic Cr metal, where flat (i.e. 1D) parts of the Fermi surface give rise to an nesting induced spin density wave. [8] Another example is the superconductor Sr_2RuO_4, which dispite its tetragonal symmetry has flat one dimensional sheets of Fermi surface that give rise to nesting induced peaks in its susceptibility. [9, 10] Generally, these cases are large Fermi surface metals, which are not of interest as thermoelectrics. However, there is no symmetry or other fundamental reason that this must always be the case and we begin by pointing out counterexamples.

The face centered cubic rocksalt structure chalcogenides, PbTe, PbSe, PbS and SnTe are the basis of excellent thermoelectric materials. [1, 2] While the thermoelectric properties of these materials has been discussed in terms of various physical models, band structure calculations in combination with standard Boltzmann transport theory can reproduce and predict their thermopowers, as illustrated by predictions for PbSe. [12, 13] As is well known, the valence band (p-type) electronic structure is dominated by L-point hole pockets for low carrier concentrations and T, while at higher carrier concentrations and T transport and other data imply additional electronic features, often discussed as a second heavy band. [14–16] According to band structure calculations, there is no second heavy band, but instead connections develop between the L-point pockets near but not at the valence band maximum.

This is illustrated in Fig. 1, which shows energy isosurfaces for the near valence band edge of PbTe, PbSe, PbS and SnTe. These are based on calculations done with the augmented planewave plus local orbital method, [17] as implemented in the WIEN2k code. [18] The calculations included spin-orbit, which is needed for these materials. We employed

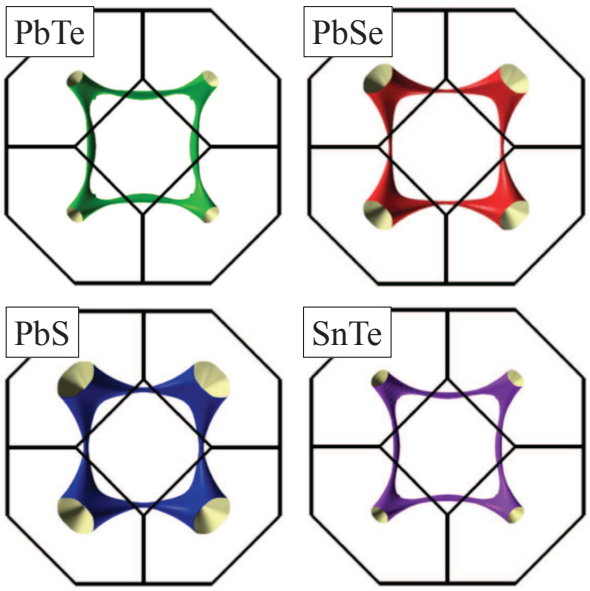

FIG. 1. (color online) Calculated valence band constant energy surfaces of PbTe, PbSe, PbS and SnTe, at 0.25 eV, 0.49 eV, 0.61 eV, and 0.41 eV below the valence band maximum, respectively. The corresponding carrier concentrations in holes per unit cell are 0.005, 0.030, 0.054 and 0.016, respectively.

the modified Becke-Johnson potential of Tran and Blaha (TB-mBJ), [19] which generally gives improved band gaps for simple semiconductors and insulators. [19–21] Besides these details the calculations are similar to those presented previously. [12, 22–30] The densities of states (not shown) show low values characteristic of a light band up to the energy where the L-point pockets connect, at which point there is a sharp onset of a steeply rising density of states, which is clearly beneficial for obtaining enhanced $S(T)$ at doping levels near the onset and was discussed in the context of the thermoelectric performance of PbTe. [27] Here we associate this with the pipes.

Qualitatively, the Fermi surface of a doped superlattice or other 2D semiconductor is cylindrical running along the stacking direction. The conductivity is low along the cylinder and high in the plane. Considering for example the conductivity along x for a cubic network of pipes running along k_x, k_y and k_z as is approximately the case in these materials, the pipes along k_y and k_z will contribute as in a superlattice material in plane, while the pipes along k_x will behave like the stacking direction and will not contribute to the conductivity. Thus the energy dependence and other behavior will be the same as the superlattice, including the enhanced 2D behavior of the thermopower, except that now the properties will be isotropic due to the cubic symmetry and superposition of pipes on different directions.

Clearly, the electronic structures of the chalcogenides shown in Fig. 1 are approximations of this idealized behavior. Nonetheless, they suggest elucidation of the behavior of a cubic or other three dimensional semiconductor with a low dimensional electronic structure in the sense discussed above. We suggest that this may be a useful paradigm in the search for new high performance thermoelectric materials.

CALCULATIONS

To describe the behavior of the transport in the aforementioned "pipes" scenario, we pursue some calculations to elucidate the relevant physics. We consider the case of a one band material with a pipe-like electronic structure. We begin with the assumption that the electronic scattering time $\tau(E)$ is independent of energy, i.e. the "constant scattering time approximation" (CSTA). The CSTA has been used with quantitative accuracy to describe the thermopower of a substantial number of thermoelectric materials [27, 31–38] so that its usage is on solid practical grounds.

Then we have the canonical expressions for the electrical conductivity $\sigma(T)$ and Seebeck coefficient $S(T)$:

$$\sigma(E) = N(E)v^2(E)\tau(E) \quad (1)$$

$$\sigma(T) = -\int_{-\infty}^{\infty} dE\sigma(E)df(E-\mu)/dE \quad (2)$$

$$S(T) = -\frac{k_B}{e\sigma(T)}\int_{-\infty}^{\infty} dE\sigma(E)\frac{E-\mu}{T}df(E-\mu)/dE \quad (3)$$

where f is the Fermi function, e the electronic charge, k_B is Boltzmann's constant, $\tau(E)$ is the scattering time, $v(E)$ the Fermi velocity, μ the chemical potential and $N(E)$ the density of states. The tensor indices are suppressed for clarity, and in addition the integrations in actual calculations involve a Brillouin-zone sum.

We now compare the thermopower and power factor $S^2\sigma$ of two specific idealized Fermi surface topologies: a two dimensional cylindrical Fermi surface connecting the L-points of the fcc Brillouin zone, as suggested by Figure 1, and a three dimensional spherical Fermi surface. This is an idealization, as in an actual material Fermi surfaces which contact Brillouin zone faces must do so at perpendicular angles, so that the pipes must reconnect at the L-point pockets, as they do in, for example, band structure calculations for PbTe. Both bands are assumed to be parabolic, and to ensure a fair comparison we choose the radial mass of the cylinder and of the sphere to be equal. Additionally, as was noted by Ref. 39, in the chalcogenides the cylindrical band is twelve-fold degenerate and we have assumed this here. For comparison purposes we have assumed the spherical Fermi surface to also be twelve-fold degenerate.

Then within the CSTA the above integrals are easily evaluated for both the 3D and 2D cases, yielding the following

expressions (here $\eta = \mu/T$, the reduced chemical potential.)

$$S_{3D}(T) = \frac{5}{3}\frac{F_{3/2}(\eta)}{F_{1/2}(\eta)} - \eta \quad (4)$$

$$\sigma_{3D}(T) = \frac{pe^2\tau}{m^*} \quad (5)$$

$$S_{2D}(T) = 2\frac{F_1(\eta)}{F_0(\eta)} - \eta \quad (6)$$

$$\sigma_{2D}(T) = \frac{2pe^2\tau}{3m^*} \quad (7)$$

Here p is the carrier density given as

$$p = \int dE N(E) f(E-\mu) \quad (8)$$

where $N(E)$ is the density of states, m^* the carrier effective mass, and F is the Fermi-Dirac integral, defined as

$$F_i(\eta) = \int_0^\infty x^i/(\exp(x-\eta)+1) \quad (9)$$

The 2/3 factor for the two-dimensional conductivity arises because, each of the cylinders contributing to the density-of-states, and hence p, conducts in only two of three directions. The final piece of information necessary to calculate the thermopower is the relation of the reduced chemical potential η to the carrier concentration p, which is done (for each of the two cases) by inverting Eq. 8; details of this procedure can be found in Ref. 44.

With these mathematical preliminaries completed, we now move to the calculated results. For concreteness (although the results do not sensitively depend on these assumptions) we have assumed an fcc cell of lattice constant 6.46 Å, band masses of 0.2 m_0, where m_0 is the free electron mass, and fixed the temperature at 1000 K. This is the approximate maximum operating temperature of the chalcogenides. For the electrical conductivity we have assumed a doping independent scattering time τ of 10^{-15} sec, which yields high temperature conductivities of 100 - 1000 $(\Omega\text{-cm})^{-1}$, in line with experimental results on these materials. In Figure 2 we present the calculated thermopower results for the two scenarios. As is evident, the 2D thermopower exceeds the 3D values by a substantial margin throughout the entire range from 0.001 - 0.5 holes/unit cell. At the heavy dopings of 0.05 - 0.1 per unit cell, the 2D thermopower is nearly double the 3D value, which is highly favorable for thermoelectric performance, and this thermopower increase comes at a conductivity reduction (Eqs. 5 and 7), relative to the 3D case, of only one third. Given this, it is not surprising that the calculated 2D power factor (Figure 3) exceeds that of the 3D case across the entire range of concentration modeled, and its maximum value is two and a half times the corresponding 3D maximum. It is highly likely that correspondingly higher 2D performance (i.e. ZT), relative to the 3D case, would also occur. We emphasize that the notation 2D and 3D is to distinguish the cases, but that in both cases we are referring to the bulk, macroscopic measurable values for the cubic crystal.

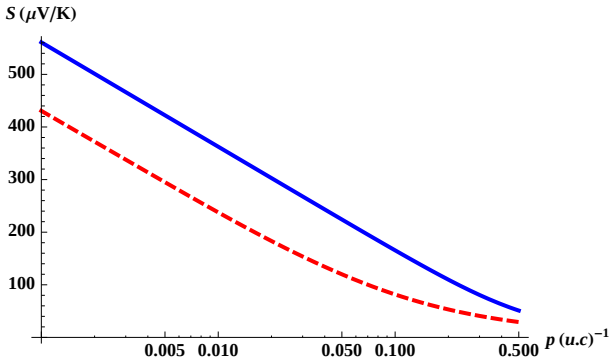

FIG. 2. (color online) The calculated thermopower for the 2D (blue solid line) and 3D (red dashed line) cases. Carrier concentrations are given in carriers per unit cell.

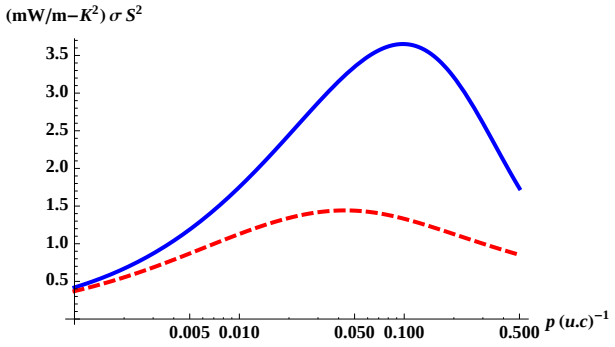

FIG. 3. (color online) The calculated power factor $S^2\sigma$ in mW/m-K^2 for the 2D (blue solid line) and 3D (red dashed line) cases.

ANALYSIS OF ENHANCED SEEBECK COEFFICIENT IN 2D CASE

The results of the previous section strongly suggest that the two dimensional "pipe" topology is favorable for thermoelectric performance, particularly for the Seebeck coefficient, an indispensable ingredient of good thermoelectric performance. Here we provide analytic understanding of this result.

To a first approximation, the enhanced behavior of the 2D system modeled here can be traced to the relatively larger Fermi surface volume (or, equivalently, carrier concentration) of a 2D cylinder relative to a 3D sphere, for given Fermi energy. In this case the Fermi surface volume of the cylinder is proportional to the length of the cylinder $= \frac{2\pi}{a}$, which is a value much larger than the radius of the cylinder or the sphere, so that for given Fermi energy the carrier concentration is much larger. The Fermi energy is relevant because of the well-known Mott formula for the thermopower,

$$S = \frac{\pi^2 k_B}{3e} k_B T d\log(\sigma(E))/dE_{|E=E_F} \quad (10)$$

and for a parabolic 3D band yields

$$S = \frac{\pi^2 k_B}{2e} k_B T/E_F \quad (11)$$

so that the thermopower is inversely proportional to the Fermi energy. In two dimensions, at fixed carrier concentration the Fermi energy is much smaller than in three dimensions, and the thermopower is enhanced as a result.

To gain additional insight into this phenomenon, as well as explore the effect of changing parameters such as the effective mass and temperature, we now pursue analytic calculations within two well-known limits for which closed form results are available: the degenerate limit, when $\eta \equiv E_F/T \gg 1$, and the non-degenerate limit, when $\eta < 0$. High thermoelectric performance is typically found somewhat between these two regimes, but together these regimes account for most of the behavior of the thermopower in Figure 1. We begin with the degenerate limit. In two dimensions, for radial mass m^*, using the Mott formula it is easy to show (assuming a band degeneracy of 24, 2 for spin and 12 for the 12 "pipes") that the thermopower takes the form

$$S_{2D} = \frac{\pi^2}{3}\frac{k_B}{e}\frac{3m^* a^2 k_B}{\pi\hbar^2 p} \tag{12}$$

where p is the carrier concentration per unit cell, and similarly for 3D (assuming the same band degeneracy)

$$S_{3D} = \frac{\pi^2}{2}\frac{k_B}{e}\frac{2m^* a^2 k_B T}{\hbar^2(\pi^2 p)^{\frac{2}{3}}} \tag{13}$$

so that one finds the simple result that

$$S_{2D}/S_{3D} = (\pi/p)^{\frac{1}{3}} \tag{14}$$

Since the carrier concentration p per unit cell is typically much less than unity, one finds S_{2D} to be substantially larger than S_{3D}. Note also that for large unit cells, one requires proportionately greater carrier concentrations *per cell* to keep the same carrier concentration *per cubic centimeter*, so that for larger cells the above equation has a smaller range of validity. Numerically for p=0.5/u.c. (yielding an η_{2D} of 5.5) this ratio is 1.845, while the exact result is 1.747, less than a 6 percent difference.

To treat the non-degenerate limit, we note that in this limit thermopower is generally logarithmic in carrier concentration (the straight lines in Figure 1), so it is the prefactors that are at issue. The non-degenerate limit is typically specified by $\eta \ll 0$, so that the Fermi function $(\exp(\frac{E-\mu}{T})+1)^{-1}$ reduces simply to $\exp\frac{\mu-E}{T}$ and the integrals involving the Fermi function can be done exactly. In this limit, as is well known [45], the three dimensional parabolic band thermopower is given by

$$S(p,T)_{3D} = \frac{k_B}{e}(\frac{5}{2} - \eta_{3D}(p,T)) \tag{15}$$

It is a simple matter to work out the corresponding value for our 2D cylindrical parabolic band and one finds that

$$S(p,T)_{2D} = \frac{k_B}{e}(2 - \eta_{2D}(p,T)) \tag{16}$$

Note that η_{2D} and η_{3D} vary due to the topology difference, and we now work out an expression for their difference. For 2 dimensions, the relation of η and p can be evaluated easily and is simply (for all temperatures)

$$\eta_{2D} = \log(\exp(\frac{\pi p}{3m^* T a^2}) - 1) \tag{17}$$

and in the non-degenerate limit this becomes simply

$$\eta_{2D} = \log(\frac{\pi p}{3m^* T a^2}) \tag{18}$$

One can similarly work out an expression for η_{3D} in the non-degenerate limit and one finds

$$\eta_{3D} = \log\left(\frac{4\pi^{3/2} p}{3(2m^*)^{\frac{3}{2}} a^3 T^{\frac{3}{2}}}\right) \tag{19}$$

so that, restoring the appropriate powers of $\hbar$ and k_B one finds that

$$\eta_{2D} - \eta_{3D} = -\log\left(\frac{m^{*1/2} a (k_B T)^{\frac{1}{2}}}{\sqrt{2\pi}\hbar}\right) \tag{20}$$

For the modeled situation ($m^* = 0.2m_0, T = 1000K, a =$ 6.46Å) the difference is -2.097 so that in the non-degenerate limit one finds $S_{2D} - S_{3D} = 1.597 k_B/e = 137\mu V/K$, which is very close to the difference in these values at the left hand of Figure 1. This is a substantial increase, needless to say.

The last equation reveals that if the effective mass (which was chosen on the basis of effective masses in the chalcogenides and Bi_2Te_3) is larger, the effective benefit in the non-degenerate limit is smaller, but for large effective mass materials one is typically closer to the degenerate limit. Conversely, if the temperature is smaller (such as for room temperature applications) the difference is correspondingly greater, provided the sample remains in the non-degenerate limit.

SUMMARY AND CONCLUSIONS

To summarize, we have here shown that (1) low dimensional electronic structures can occur even in cubic semiconductors, and that (2) such electronic structures are highly beneficial for thermoelectric performance. This represents a new paradigm for high thermoelectric performance: *low-dimensional* electronic structures enhancing performance in fully *three dimensional bulk* thermoelectrics. We suggest searching for new thermoelectric materials among such compounds. One such compound may be SnTe [46, 47].

Acknowledgment

This research was supported by the U.S. Department of Energy, EERE, Vehicle Technologies, Propulsion Materials Program (DP), the Solid State Solar-Thermal Energy Conversion Center (S3 TEC), an Energy Frontier Research Center funded by the US Department of Energy, Office of Science, Office of Basic Energy Sciences under Award Number: de-sc0001299/DE-FG02-09ER46577 (XC,DJS).

[1] A.F. Ioffe, *Semiconductor Thermoelements and Thermoelectric Cooling* (Inforesearch, London, 1957).
[2] C. Wood, Rep. Prog. Phys. **51**, 459 (1988).
[3] J. M. Ziman, *Electrons and Phonons*, (Oxford Univ. Press: New York), 2001.
[4] W. Jones and N. H. March, *Theoretical Solid State Physics*, (Courier Dover Publications), 1985.
[5] L.D. Hicks and M.S. Dresselhaus, Phys. Rev. B **47**, 16631 (1993).
[6] I. Terasaki, Y. Sassago and K. Uchinokura, Phys. Rev. B **56**, 12685 (1997).
[7] D.J. Singh, Phys. Rev. B **61**, 13397 (2000).
[8] E. Fawcett, Rev. Mod. Phys. **60**, 209 (1988).
[9] I. I. Mazin and D. J. Singh, Phys. Rev. Lett. **82**, 4324 (1999).
[10] Y. Sidis, M. Braden, P. Bourges, B. Hennion, S. Nishizaki, Y. Maeno and Y Mori, Phys. Rev. Lett. **83**, 3320 (1999).
[11] D.J. Singh and L. Nordstrom, *Planewaves Pseudopotentials and the LAPW Method, 2nd Edition*, (Springer:Berlin), 2006.
[12] D. Parker and D.J. Singh, Phys. Rev. B **82**, 035204 (2010).
[13] Q. Zhang, F. Cao, W. Liu, K. Lukas, B. Yu, S. Chen, C. Opeil, D. Broido, G. Chen and Z. Ren. J. Am. Chem. Soc. **134**, 10031 (2012).
[14] Y. I. Ravich, B. A. Efimova and V. I. Tamarchenko, Phys. Stat. Sol. B **48**, 11 (1971).
[15] Y. I. Ravich, B. A. Efimova and V. I. Tamarchenko. Phys. Stat. Sol. B **48**, 453 (1971).
[16] C. E. Ekuma, D. J. Singh, J. Moreno and M. Jarrell, Phys. Rev. B **85**, 085205 (2012).
[17] E. Sjostedt, L. Nordstrom and D. J. Singh, Solid State Comm. **114**, 15 (2000).
[18] P. Blaha, K. Schwarz, G. K. H. Madsen, D. Kvasnicka and J. Luitz, WIEN2k, An Augmented Plane Wave + Local Orbitals Program for Calculating Crystal Properties (Karlheinz Schwarz, Techn. Universität Wien, Austria), 2001. ISBN 3-9501031-1-2.
[19] F. Tran and P. Blaha, Phys. Rev. Lett. **102**, 226401 (2008).
[20] D. J. Singh, Phys. Rev. B **82**, 205102 (2010).
[21] D. Koller, F. Tran and P. Blaha, Phys. Rev. B **83**, 195314 (2011).
[22] P.J. Lin and L. Kleinman, Phys. Rev. **142**, 478 (1966).
[23] S.H. Wei and A. Zunger, Phys. Rev. B **55**, 13605 (1997).
[24] D.I. Bilc, S.D. Mahanti and M.G. Kanatzidis, Phys. Rev. B **74**, 125202 (2006).
[25] K. Hummer, A. Gruneis and G. Kresse, Phys. Rev. B **75**, 195211 (2007).
[26] L. Zhang, A. Grystiv, P. Rogl, E. Bauer and M. Zehetbauer, J. Phys. D **42**, 225405 (2009).
[27] D.J. Singh, Phys. Rev. B **81**, 195217 (2010).
[28] L. Q. Xu, Y.P. Zheng and J.C. Zheng, Phys. Rev. B **82**, 195102 (2010).
[29] A. Svane, N.E. Christensen, M. Cardona, A.N. Chantis, M. van Schilgaarde and T. Kotani, Phys. Rev. B **81**, 245120 (2010).
[30] D. J. Singh. Func. Mat. Lett. **3**, 223 (2010).
[31] G.K.H. Madsen, K. Schwarz, P. Blaha and D.J. Singh, Phys. Rev. B **68**, 125212 (2003).
[32] L. Zhang, M.-H. Du and D.J. Singh, Phys. Rev. B **81**, 075117 (2010).
[33] K.P. Ong, D.J. Singh and P. Wu, Phys. Rev. B **83**, 115110 (2011).
[34] D. J. Singh and I. I. Mazin, Phys. Rev. B **56**, R1650, (1997).
[35] T. J. Scheidemantel, C. Ambrosch-Draxl, T. Thonhauser, J. V. Badding, and J. O. Sofo, Phys. Rev. B **68**, 125210, (2003).
[36] L. Bertini and C. Gatti, J. Chem. Phys. **121**, 8983, (2004).
[37] L. Lykke, B. B. Iversen, and G. K. H. Madsen, Phys. Rev. B **73**, 195121, (2006).
[38] Y. Wang, X. Chen, T. Cui, Y. Niu, Y. Wang, M. Wang, Y. Ma, and G. Zou, Phys. Rev. B **76** , 155127, (2007).
[39] Y. Pei, X. Shi, A. LaLonde , H. Wang, L. Chen and G. J. Snyder, Nature **473**, 66, 2011.
[40] K. Biswas, J. He, I.D. Blum, C-I Wu, T.P. Hogan, D.N Seidman, V.P. Dravid and M.G. Kanalzidis, Nature **489**, 414 (2012).
[41] L.D. Zhao, J. He, S. Hao, C.-I. Wu, T.P. Hogan, C. Wolverton, V.P. Dravid and M.G. Kanatzidis, J. Am. Chem. Soc. **134**, 16327 (2012).
[42] G. K. H. Madsen and D.J. Singh, Comput. Phys. Comm. **175**, 67 (2006).
[43] J. P. Perdew, K. Burke and M. Ernzerhof, Phys. Rev. Lett. **77**, 3865 (1996).
[44] J.S. Blakemore, Solid State Electronics **25**, 1067 (1982).
[45] G.S. Nolas, J. Sharp and H.J. Goldsmid, *Thermoelectrics: Basic Principles and New Materials Developments*, (Srpinger: Berlin), 2001.
[46] P.B. Littlewood, B. Mihaila, R.K. Schulze, D.J. Safarik, J.E. Gubernatis, A. Bostwick, E. Rotenberg, C.P. Opeil, T. Durakiewicz, J.L. Smith and J.C. Lashley, Phys. Rev. Lett. **105**, 086404 (2010).
[47] Y. Tanaka, Z. Ren, T. Sato, K. Nakayama, S. Souma, T. Takahashi, K. Segawa and Y. Ando, Nat. Phys. **8**, 800 (2012).